

Size-driven magnetic transitions in monodisperse MnO nanocrystals

Yi-Cheng Lee, Alexandre B. Pakhomov,^{a)} and Kannan M. Krishnan^{b)}

Department of Materials Science and Engineering, University of Washington, Seattle, Washington 98195, USA

(Presented 21 January 2010; received 28 October 2009; accepted 7 December 2009; published online 21 April 2010)

We report the observation of weak ferromagnetism up to $T_C \approx 250$ K and a spin-glass-like behavior at temperatures below $T_{SG} \approx 30$ K in nanoscale MnO particles. T_{SG} is considerably lower and T_C is much higher than the Néel temperature ($T_N = 122$ K) of bulk MnO. While the dominant low temperature behavior (below 30 K) may be attributed to the effects studied in this system before, such as uncompensated surface spins in antiferromagnetic particles, no manganese oxides have been observed with the Curie temperature as high as 250 K. We explain the magnetic ordering below T_C as due to indirect exchange of the type observed in dilute magnetic oxides, which can be mediated by crystal defects and/or surfaces. © 2010 American Institute of Physics. [doi:10.1063/1.3366611]

Magnetic properties of nanoparticles and thin films of ferromagnetic (FM) and antiferromagnetic (AFM) metals and oxides are known to differ from those in the bulk. Examples include Co, Fe_3O_4 , NiO, and MnO nanoparticle systems,^{1–5} where decreased magnetic transition temperatures, spin glass features, and biased hysteresis loops due to disorder and the effects of uncompensated surface spins have been discussed,^{5,6} in addition to possible spurious effects from secondary phases.⁷ On the other hand, recent experiments on transition metal-doped nonmagnetic oxides, e.g., Co-doped TiO_2 or Cr-doped ZnO show that ferromagnetic ordering can be induced between dopant ion spins mediated by structural defects,^{8–10} including surface and interface¹¹ (dilute magnetic oxides or DMOs). It is natural to suggest that similar indirect ordering can be also revealed in a transition metal oxide in paramagnetic state, provided the material is highly defected or has reduced dimensionality. In this work, the existence of such additional ferromagnetism up to 250 K is demonstrated in MnO nanoparticles.

Bulk MnO with the rock salt structure is antiferromagnetic with the Néel temperature, $T_N = 122$ K. It has been reported that nanoscale MnO particles can show FM or spin-glass-like behavior at low temperatures, attributed to uncompensated surface spin effects,^{12–14} or possible formation of Mn_3O_4 with $T_C (=43$ K) on the surface of the MnO core.⁷ Our single-phase, pure, monosized MnO nanoparticles ~ 10 nm in diameter also show anomalous behavior at low temperature. Scaling analyses point at a spin-glass-like state with the freezing temperature of ~ 30 K, which is consistent with interpretations discussed in the literature.^{15–17} However, none of the mechanisms proposed for MnO before can explain the observed high temperature ordering with $T_C \sim 250$ K. The possibility of material contamination being responsible for the FM signal was practically eliminated by comparison of samples prepared in six different syntheses

runs. All resulting samples showed high temperature FM. Crystallographic phase purity was checked with x-ray diffraction (XRD) and transmission electron microscopy (TEM) characterization, which does not completely exclude the presence of tiny quantities of secondary phases. However, no Mn–O phase has been reported FM or AFM in the bulk at temperatures as high as 250 K. Hence the observed ferromagnetic behavior cannot be attributed to secondary Mn–O phases.

Monodispersed MnO nanoparticles were prepared by thermal decomposition of a Mn-oleate complex in an organic solvent.¹⁸ A Mn-oleate complex was prepared by mixing 0.2 g of $\text{Mn}_2(\text{CO})_{10}$ in 2 ml of oleylamine at 100 °C. The complex solution was cooled to room temperature and then 10 ml of trioctylphosphine was added. For the growth of nanocrystals, the mixed solution was heated up to 280 °C under argon atmosphere and kept under vigorous stirring for 1 h. The reaction was then cooled to room temperature and the nanoparticles were obtained by adding ethanol, followed by centrifugation. They were then redispersed in nonpolar solvents such as hexane or toluene. TEM imaging (Fig. 1 inset) confirms that the particles are monosized with diameter ~ 10 nm. The peaks of the XRD θ - 2θ scans (Fig. 1) are indexed as single-phase MnO. Comparison with the peaks obtained for a commercial powder (Sigma-Aldrich ~ 60

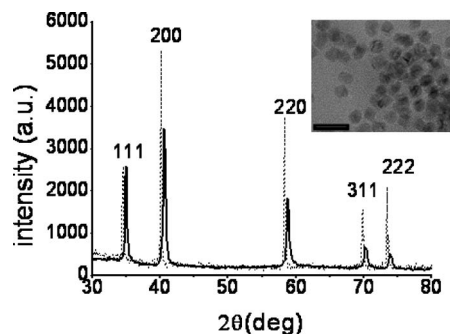


FIG. 1. XRD scan of the nanocrystals (solid line) in comparison to commercial 60-mesh MnO powders (dashed line). Inset: TEM image of manganese oxide nanocrystals. The scale bar indicates 30 nm.

^{a)}Also at NanoTech User Facility, Center for Nanotechnology, University of Washington, Seattle, WA 98195.

^{b)}Author to whom correspondence should be addressed. Electronic mail: kannanmk@u.washington.edu.

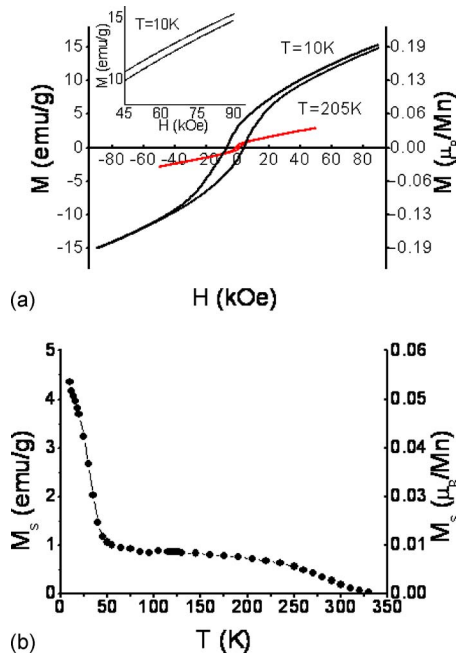


FIG. 2. (Color online) (a) Hysteresis loops of MnO nanoparticles measured at 10 and 205 K. The inset shows the enlarged part of the 10 K curve at high positive fields. (b) The temperature dependence of spontaneous magnetization of MnO nanoparticles.

mesh) shows that the lattice constant in our nanoparticles is decreased by 1.05%, apparently due to surface relaxation.

DC and AC ($100 \text{ Hz} \leq f \leq 10 \text{ kHz}$) magnetic moments were measured in the Quantum Design physical properties measurement system. Magnetization curves were measured in fields up to 90 kOe over the temperature range from 10 to 330 K and showed spontaneous magnetization and hysteresis up to $\sim 250 \text{ K}$. Figure 2(a) shows the hysteresis loops at 10 and 205 K and Fig. 2(b) shows the temperature dependence of spontaneous magnetization (M_s), where M_s has been determined by extrapolating the high-field magnetization back to $H=0$. Spontaneous magnetization [Fig. 2(b)] reduces sharply near 30 K, but remains at the level of $\sim 0.2 M_s$ (10 K) in the range ~ 50 – 250 K . In Fig. 2, magnetization is shown both in emu/g and $\mu_B/\text{Mn atom}$. Taking into account that the moment of Mn^{2+} is $5\mu_B$, we notice that only a small fraction of Mn atoms contribute to M_s : $\sim 1\%$ at $T < 30 \text{ K}$ and $\sim 0.2\%$ at $50 \text{ K} < T < 250 \text{ K}$.

The data shown in Fig. 2 reveal ferromagnetism up to 250 K, with two distinctly different types of behavior below and above ~ 30 – 40 K . The low temperature hysteresis has been observed in MnO nanoparticles before⁷ and is analyzed in some details below. However, the magnetic state in the temperature range ~ 50 – 250 K is puzzling, as no bulk manganese oxide phase has magnetic ordering temperature as high as 250 K. We suggest that this ferromagnetism may be analogous to that observed in dilute magnetic oxides. In other words, part of the Mn spins are ferromagnetically aligned in the paramagnetic matrix. The difference with the conventional DMO is that in DMO the aligned moments are those of the dopant ions, while in the case of MnO nanoparticles, Mn ions themselves possess moments, and part of them are ordered even at high temperature. One point of

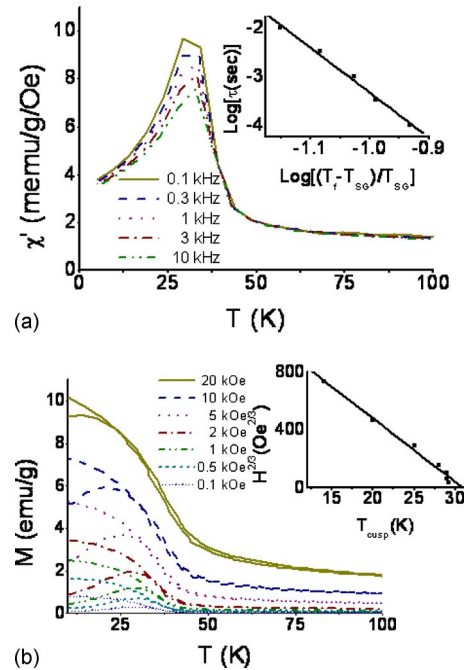


FIG. 3. (Color online) (a) The temperature dependences of the real part of AC moment at varying frequency. Inset: Vogel-Fulcher scaling plot. (b) ZFC-FC magnetization curves at varying applied fields. Inset: de AT scaling analysis, Fig. 1.

view on ferromagnetism in DMO is that it is mediated by crystal defects,^{8–11,19,20} surface being one important case.¹¹ Extending this concept to MnO allows to explain why FM can be observed in nanoparticles and is absent in bulk MnO.

In the hysteresis loop measured at 10 K, after field cooling in 90 kOe, shown in Fig. 2(a) the coercivity is large—about 6.8 kOe—and the loop is displaced by about 1310 Oe along the ordinate. The hysteresis loop is not closed at +9 T [Fig. 2(a) inset]. Similar features can be observed in spin glasses; so we performed a more detailed study showing that the low temperature properties of MnO nanoparticles indeed fit the spin glass models. Figure 3(a) shows the temperature dependences of AC susceptibility ($100 \text{ Hz} \leq f \leq 10 \text{ kHz}$). In the Ising model of a spin glass, the relaxation time follows the relation: $\tau = \tau_0 [(T_f - T_{SG})/T_{SG}]^{-z\nu}$, where $\tau \propto f^{-1}$ and the critical exponent $z\nu$ typically ranges from 7 to 10.^{21–23} T_{SG} is the critical temperature for spin glass ordering which is equivalent to the freezing temperature $T_f(f)$ at $f \rightarrow 0$, and τ_0 is the characteristic time scale for spin dynamics. In our case, the Vogel-Fulcher scaling analysis²⁴ gives $T_{SG} = 29.5 \text{ K}$, the scaling exponent $z\nu \sim 9.2$ and $\tau_0 \sim 10^{-12}$ [Fig. 3(a) inset], in reasonable agreement with the model and prior experimental results for spin glasses. Further evidence in favor of the spin glass behavior below $T_{SG} \sim 30 \text{ K}$ in MnO nanoparticles follows from the de Almeida-Thouless (AT) scaling analysis on the zero-field-cooled and field-cooled (ZFC-FC) DC magnetization measurements at varying applied fields [Fig. 3(b)]. The data fits well [Fig. 3(b) inset] to the AT equation²⁵ $H = A_{AT} (1 - \{T_f(H)/[T_f(0)]\})^{3/2}$, where $T_f(H)$ is the field-dependent freezing temperature, with $T_f(0) = 30.92 \text{ K}$, close to the Vogel-Fulcher scaling result. Yet another indication of spin-glass dynamics could be the value of relative shift of the freezing temperature per decade of frequency,

$\Delta T_f/[T_f(\Delta \log f)]$, which varies in the range of 0.004–0.018 for spin-glass systems, while for superparamagnets it is of the order of 0.3.^{26,27} The result for our samples (0.023) does not provide additional conclusive evidence. However, with a high degree of reliability, we do observe spin-glass-like behavior in this temperature range. Whether it is a true spin glass state of uncompensated surface spins, or spin-glass-like behavior due to dipolar interactions between ferromagnetic nanoscale particles remains unclear.

In conclusion, the main result of this work is the observation of a ferromagnetic state with the Curie temperature $T_C \sim 250$ K, considerably higher than the Néel temperature of bulk MnO. This observation is explained using a hypothesis that defect-(surface-)mediated indirect exchange, similar to that found in dilute magnetic oxides, is possible in transition metal oxide nanoparticles. The second property of this system—low temperature hysteretic magnetization which has been reported before—is found to have features of a spin glass with the transition temperature $T_{SG} \approx 30$ K. The small size of the particles is responsible for both the low temperature spin-glass and high temperature ferromagnetic effects in MnO.

This work has been supported by NSF/DMR Grant No. 0501421 and the NINDS, NIH intramural research program. TEM and HRTEM images were obtained at the University of Washington NanoTech User Facility, a member of the NSF National Nanotechnology Infrastructure Network (NNIN).

¹V. F. Puentes and K. M. Krishnan, *IEEE Trans. Magn.* **37**, 2210 (2001).

²A. B. Pakhomov, Y. P. Bao, and K. M. Krishnan, *J. Appl. Phys.* **97**, 10Q305 (2005).

³K. M. Krishnan, A. B. Pakhomov, Y. Bao, P. Blomqvist, Y. Chun, M. Gonzales, K. Griffin, X. Ji, and B. K. Roberts, *J. Mater. Sci.* **41**, 793 (2006).

⁴M. Gonzales and K. M. Krishnan, *J. Magn. Magn. Mater.* **293**, 265 (2005).

⁵R. H. Kodama, S. A. Makhlof, and A. E. Berkowitz, *Phys. Rev. Lett.* **79**,

1393 (1997).

⁶D. T. Margulies, F. T. Parker, F. E. Spada, R. S. Goldman, J. Li, R. Sinclair, and A. E. Berkowitz, *Phys. Rev. B* **53**, 9175 (1996).

⁷A. E. Berkowitz, G. F. Rodriguez, J. I. Hong, K. An, T. Hyeon, N. Agarwal, D. J. Smith, and E. E. Fullerton, *Phys. Rev. B* **77**, 024403 (2008).

⁸K. A. Griffin, A. B. Pakhomov, C. M. Wang, S. M. Heald, and K. M. Krishnan, *J. Appl. Phys.* **97**, 10D320 (2005).

⁹T. C. Kaspar, S. M. Heald, C. M. Wang, J. D. Bryan, T. Droubay, V. Shutthanandan, S. Thevuthasan, D. E. McCready, A. J. Kellock, D. R. Gamelin, and S. A. Chambers, *Phys. Rev. Lett.* **95**, 217203 (2005).

¹⁰M. Venkatesan, C. B. Fitzgerald, J. G. Lunney, and J. M. D. Coey, *Phys. Rev. Lett.* **93**, 177206 (2004).

¹¹B. K. Roberts, A. B. Pakhomov, P. Voll, and K. M. Krishnan, *Appl. Phys. Lett.* **92**, 162511 (2008).

¹²G. H. Lee, S. H. Huh, J. W. Jeong, B. J. Choi, S. H. Kim, and H. C. Ri, *J. Am. Chem. Soc.* **124**, 12094 (2002).

¹³W. S. Seo, H. H. Jo, K. Lee, B. Kim, S. J. Oh, and J. T. Park, *Angew. Chem., Int. Ed.* **43**, 1115 (2004).

¹⁴M. A. Morales, R. Skomski, S. Fritz, G. Shelburne, J. E. Shield, M. Yin, S. O'Brien, and D. L. Leslie-Pelecky, *Phys. Rev. B* **75**, 134423 (2007).

¹⁵A. E. Berkowitz, G. F. Rodriguez, J. I. Hong, K. An, T. Hyeon, N. Agarwal, D. J. Smith, and E. E. Fullerton, *J. Phys. D: Appl. Phys.* **41**, 134007 (2008).

¹⁶C. Djurberg, P. Svedlindh, P. Nordblad, M. F. Hansen, F. Bodker, and S. Morup, *Phys. Rev. Lett.* **79**, 5154 (1997).

¹⁷M. Osth, D. Herisson, P. Nordblad, J. A. De Toro, and J. M. Riveiro, *J. Magn. Magn. Mater.* **313**, 373 (2007).

¹⁸J. Park, E. A. Kang, C. J. Bae, J. G. Park, H. J. Noh, J. Y. Kim, J. H. Park, J. H. Park, and T. Hyeon, *J. Phys. Chem. B* **108**, 13594 (2004).

¹⁹K. A. Griffin, A. B. Pakhomov, C. M. Wang, S. M. Heald, and K. M. Krishnan, *Phys. Rev. Lett.* **94**, 157204 (2005).

²⁰K. Griffin Roberts, M. Varela, S. Rashkeev, S. T. Pantelides, S. J. Pennycook, and K. M. Krishnan, *Phys. Rev. B* **78**, 014409 (2008).

²¹A. T. Ogielski, *Phys. Rev. B* **32**, 7384 (1985).

²²S. Kirkpatrick and D. Sherrington, *Phys. Rev. B* **17**, 4384 (1978).

²³I. A. Campbell, *Phys. Rev. B* **33**, 3587 (1986).

²⁴K. Gunnarsson, P. Svedlindh, P. Nordblad, L. Lundgren, H. Aruga, and A. Ito, *Phys. Rev. Lett.* **61**, 754 (1988).

²⁵J. R. L. de Almeida and D. J. Thouless, *J. Phys. A* **11**, 983 (1978).

²⁶J. A. Mydosh, *Spin Glasses: An Experimental Introduction* (Taylor & Francis, London, 1993).

²⁷C. A. M. Mulder, A. J. Vanduyneveldt, and J. A. Mydosh, *Phys. Rev. B* **23**, 1384 (1981).